

Scanning Force Microscopy of *Escherichia coli* RNA Polymerase · σ^{54} Holoenzyme Complexes with DNA in Buffer and in Air

Alexandra Schulz, Norbert Mücke, Jörg Langowski and Karsten Rippe*

Deutsches
Krebsforschungszentrum
Abteilung Biophysik der
Makromoleküle
Im Neuenheimer Feld 280
D-69120 Heidelberg, Germany

Scanning force microscopy (SFM) was used to visualize complexes of *Escherichia coli* RNA polymerase · σ^{54} (RNAP · σ^{54}) and a 1036 base-pair linear DNA fragment containing the *glnA* promoter. In order to preserve the native hydration state of the protein-DNA complexes, the samples were injected directly into the SFM fluid cell and imaged in buffer. With this protocol, an apparent bending angle of $26(\pm 34)^\circ$ was determined for the specific complexes at the promoter. The bending angle of the unspecifically bound RNAP · σ^{54} showed a somewhat broader distribution of $49(\pm 48)^\circ$, indicating the existence of conformational differences as compared to the closed complex. In about two-thirds of the closed complexes, the RNA polymerase holoenzyme was located in a lateral position with respect to the DNA and the bend of the DNA was pointing away from the protein. This conformation was consistent with the finding that for the complexes at the promoter, the apparent contour length was reduced by only about 6 nm in buffer as compared to the free DNA. From these results we conclude that in the closed complex of RNAP · σ^{54} , the DNA was not wrapped around the polymerase, and we present a model for the trajectory of the DNA with respect to the RNA polymerase. The images acquired in buffer were compared to samples that were washed with water and then dried before imaging. Two artefacts of the washing and drying process were detected. First, extensive washing of the sample reduced the number of the specific complexes bound at the promoter (closed complex of RNAP · σ^{54}) from about 70% to 30%. This is likely to be a result of sliding of the RNAP · σ^{54} holoenzyme along the DNA induced by the washing process. Second, the apparent DNA shortening of the contour length of RNAP · σ^{54} -DNA complexes at the promoter as compared to the contour length of the free DNA was 22 nm for the dried samples as opposed to only 6 nm for the undried samples imaged in buffer. This suggests an artefact of the drying process.

© 1998 Academic Press

Keywords: protein-DNA interaction; transcription; RNA polymerase; atomic force microscopy; tapping in fluid

*Corresponding author

Introduction

Gene expression in *Escherichia coli* starts with the specific binding of RNA polymerase at the promoter. This step has been designated as closed com-

plex formation. To initiate transcription, the closed complex of the polymerase has to be converted into the open complex, which is characterized by strand separation of the DNA double helix in the promoter region. For *E. coli* RNA polymerase complexed with the σ^{54} factor (RNAP · σ^{54}), this process requires a specific promoter consensus sequence and interaction with activator proteins like, for example, NtrC (nitrogen regulatory protein C, also designated as NR₁) that are mediated by DNA-looping (Collado-Vides *et al.*, 1991; North *et al.*,

Abbreviations used: SFM, scanning force microscopy; RNAP, RNA polymerase; NtrC, nitrogen regulatory protein C; EM, electron microscopy.

E-mail address of the corresponding author: Karsten.Rippe@dkfz-heidelberg.de

1993; Reitzer & Magasanik, 1986; Rippe *et al.*, 1997a). Upon hydrolysis of ATP, the activator protein catalyzes the transition of RNAP· σ^{54} from the closed complex to the open complex. This is an important difference from the standard holoenzyme form of *E. coli* RNA polymerase, the RNA polymerase· σ^{70} holoenzyme (RNAP· σ^{70}), which can initiate open complex formation from a promoter without the interaction with an additional activator protein and/or hydrolysis of ATP. A separate analysis of the closed complex of RNAP· σ^{70} *in vitro* requires a temperature of 0 to 4°C, which prevents the transition to the open complex, whereas at room temperature a mixture of closed and open complexes is present (Schickor *et al.*, 1990). For RNAP· σ^{54} , the selective analysis of the closed complex can be done at ambient temperature, because the formation of the open complex would require the presence of the activator protein and ATP.

We describe the use of scanning force microscopy (SFM, also termed atomic force microscopy or AFM) to study the specific closed complexes formed by RNAP· σ^{54} at the *glnA* promoter and unspecifically bound RNAP· σ^{54} . SFM can be used for imaging DNA and protein-DNA complexes without further fixing or staining, the only constraint being that the molecule is bound to a surface (for reviews, see Bustamante & Rivetti, 1996; Bustamante *et al.*, 1997; Hansma & Hoh, 1994; Lyubchenko *et al.*, 1995; Schaper & Jovin, 1996). In various studies, SFM has been used in the field of transcription (Guthold *et al.*, 1994; Kasas *et al.*, 1997; Palecek *et al.*, 1997; Rees *et al.*, 1993; Rippe *et al.*, 1997a; Wyman *et al.*, 1997). At present, the resolution of the SFM is comparable to conventional electron microscopy (EM). However, SFM is a topographic technique, so that additional information is encoded in the height of the sample. Preparation of the DNA sample for SFM imaging can be done by using Mg^{2+} to bind the DNA to the negatively charged surface of freshly cleaved mica. This process is relatively gentle and slow, and it has been shown that the DNA re-equilibrates on the substrate under the conditions of deposition used here (Rivetti *et al.*, 1996). No further treatment is required to enhance the contrast. In addition, imaging by SFM can be conducted in a wide range of biological buffer solutions. Thus, SFM offers the unique possibility to study protein-DNA complexes in their native hydration state and artefacts due to drying of the sample can be avoided.

Here, images of RNAP· σ^{54} -DNA complexes were acquired in transcription buffer and compared to those of dried samples that have been washed with water. Two artefacts of the washing and drying procedure were detected, demonstrating the advantage of imaging protein-DNA complexes in their native hydration state. Based on the images of undried RNAP· σ^{54} -DNA samples that were imaged in buffer, we have derived a model

for the trajectory of the DNA in the closed complex of RNAP· σ^{54} .

Results

Images of RNAP· σ^{54} -DNA complexes

The system studied here consisted of RNA polymerase· σ^{54} holoenzyme from *E. coli* and a 1036 base-pair linear *PvuII* fragment from pJES534 with the *glnA* promoter (Klose *et al.*, 1993). On this template the promoter is located 139 nm away from one end of the DNA and 213 nm from the other end. Upon incubation of RNAP· σ^{54} and the DNA fragment for ten minutes at 37°C in 5 mM Hepes-KOH (pH 8.0), 10 mM magnesium acetate, 50 mM potassium acetate complexes were formed that were subsequently studied by SFM. Representative images are displayed in Figure 1 (2 $\mu\text{m} \times 2 \mu\text{m}$ overviews) and in Figure 2 (600 nm \times 400 nm magnified images). The samples were prepared by using three different protocols. According to protocol I (Figures 1a and Figure 2a) the protein-DNA complexes were injected directly into the SFM fluid cell in the same buffer used for forming the complexes and bound to the mica surface *via* Mg^{2+} and Ni^{2+} . The procedure worked very reliably and is described in detail in Materials and Methods. It avoided drying the sample and is therefore regarded as the least invasive method to prepare the sample. It can be seen in Figures 1a and 2a that the quality of the images was very good. The images acquired in air were obtained after washing the samples with 1 ml of water (protocol II, Figure 1b) or with 50 ml of water (protocol III, Figure 1c). The washing step with water was required for imaging in air because residual salt, which would obscure the image, had to be removed before drying.

With all three protocols the complexes of RNAP· σ^{54} with the 1036 bp template were clearly visible. Successive images recorded at different scanning angles resulted in identical images for all three protocols used. Thus, the molecules were stably bound to the surface and an effect of the scanning direction on the observed conformation of the molecules can be excluded.

Most of the complexes that can be seen in Figure 1a and b have the RNA polymerase bound at the position corresponding to the promoter, i.e. about two-fifths away from one end of the DNA and three-fifths away from the other end. In addition some free DNA, RNAP· σ^{54} , and σ^{54} could be detected. In the quantitative analysis of the images described below, only complexes were evaluated that had a single RNAP· σ^{54} bound to the DNA and were not obstructed by other molecules. A magnification (600 nm \times 400 nm) of single complexes given in Figure 2 allowed the detailed quantitative analysis of the conformation of the complexes that is described below. The DNA imaged in fluid (Figures 1a and 2a) appeared higher (≈ 1.5 nm) than in the images obtained in

air (≈ 0.5 nm, note also the different height scales in Figure 1). This effect has been observed previously and has been attributed mostly to the

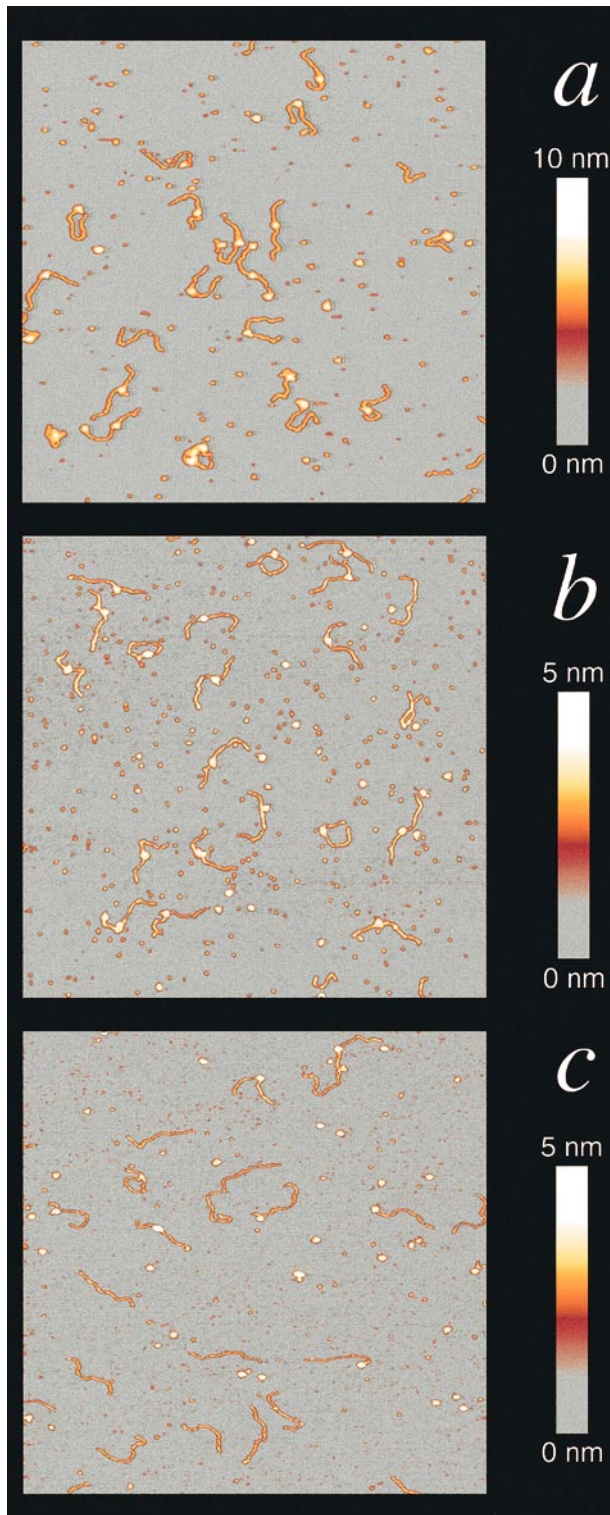


Figure 1. Complexes of RNAP· σ^{54} with DNA. The $2 \mu\text{m} \times 2 \mu\text{m}$ SFM images of a sample in buffer prepared according to protocol I (a), and in air prepared according to protocol II (b) and protocol III (c). Apart from the RNAP· σ^{54} -DNA complexes, the pictures display some free DNA fragments and free RNAP· σ^{54} .

reduced interaction of tip and DNA in aqueous solutions (see Rippe *et al.*, 1997c and references therein).

Binding positions of RNAP· σ^{54}

To distinguish between RNAP· σ^{54} bound specifically at the promoter or unspecifically at other positions of the DNA template, we determined the position of the RNAP· σ^{54} binding site on the DNA template by measuring the length of the DNA from the center of the polymerase to each end. The binding position was then expressed as the ratio r of the length of the shorter DNA tract divided by the total contour length with a calculated value of $r = 0.40$ for the location of the promoter. The distribution of the values obtained for r for the three different sample preparations is shown in Figure 3. In fluid (Figure 3a) and in air with the 1 ml wash (Figure 3b) the histogram could be described by a Gaussian distribution with mean (standard deviation) values of $r = 0.41(\pm 0.03)$ and $r = 0.39(\pm 0.04)$. The observed difference in Figure 3a and b for the mean values of r were statistically significant at the 5% level as judged from a t -test. In order to be able to differentiate between closed complexes at the promoter

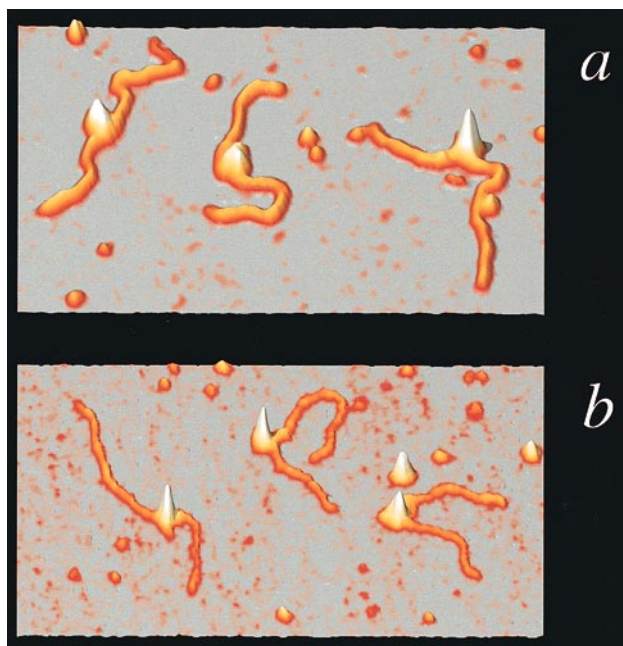


Figure 2. Magnified images of specific RNAP· σ^{54} complexes at the *glnA* promoter. According to the position of the *glnA* promoter, RNAP· σ^{54} binds in a specific complex about two-fifths away from one end of the DNA fragment. a, The $600 \text{ nm} \times 400 \text{ nm}$ SFM images of the RNAP· σ^{54} closed complex at the promoter in fluid. The DNA appears to be somewhat bigger in fluid than in air. This is due to the observed increase in the apparent DNA height. The color coding for the z-direction is the same as in Figure 1a. b, The $600 \text{ nm} \times 400 \text{ nm}$ SFM images of the RNAP· σ^{54} closed complex at the promoter in air. The color coding for the z-direction is the same as in Figure 1b.

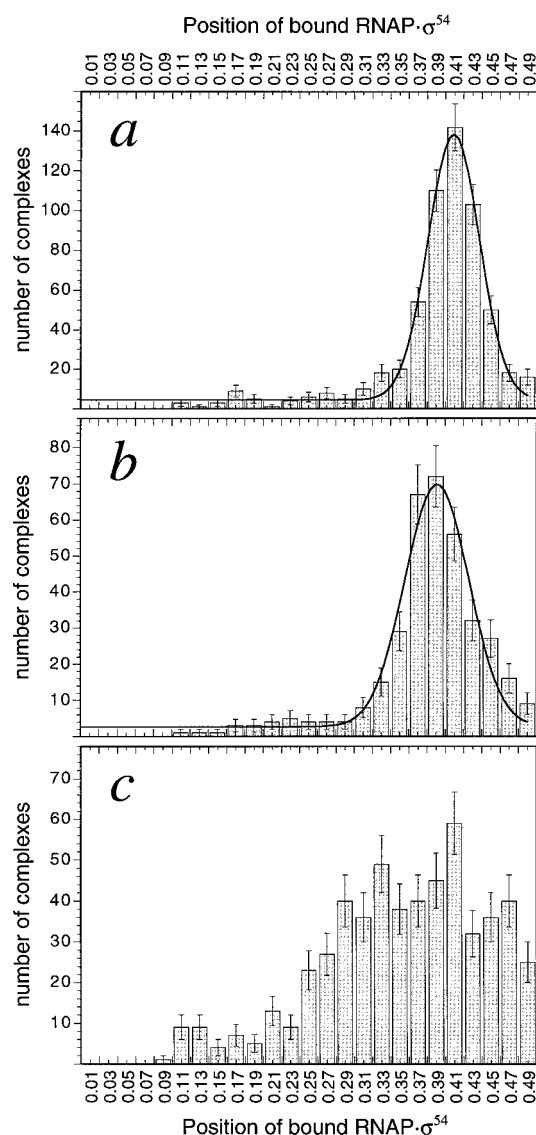


Figure 3. Histogram of the position of bound RNAP· σ^{54} . a, Histogram of the position of bound RNAP· σ^{54} in buffer (protocol I). b, Histogram of the position of bound RNAP· σ^{54} in air (1 ml wash, protocol II). c, Histogram of the position of bound RNAP· σ^{54} in air (50 ml wash, protocol III).

and unspecifically bound RNA polymerase, we designated all complexes as specific closed complexes that were within two standard deviations of the calculated value for the position of the promoter, i.e. within $r = 0.40(\pm 0.06)$. A standard deviation of 0.06 corresponds to a standard deviation of around 20 nm for the measurement of the DNA contour length. This value was in the range of the standard deviation measured for the total contour length of the protein-DNA complexes of 14 to 26 nm (see Table 4). Thus, the width of the observed distribution of the binding positions in Figure 3a and b around the position of the promoter is likely to reflect mostly the accuracy of the length measurements. According to the above cri-

terion of $r = 0.40(\pm 0.06)$, we observed about 70 and 68% specific complexes for the samples prepared according to protocol I and II, respectively, and about 30% unspecific complexes. A large number of the unspecific complexes (13% and 11% of the total number of complexes) had the polymerase bound at the ends of the DNA fragment.

When the sample was extensively washed with 50 ml of water (Figure 3c), a rather broad distribution without a defined peak was observed. It appeared that strong washing of the mica destroyed the specifically bound closed complex of RNAP· σ^{54} at the promoter and led to an increased number of unspecific complexes at other positions on the template. According to the criterion for specific binding defined above, the number of specific complexes was reduced from $\approx 70\%$ to $\approx 30\%$ due to extensive washing of the samples in air (Table 1). A similar effect was observed for images scanned in fluid: when several milliliters of transcription buffer were flushed through the fluid cell at a relatively high flow-rate, the number of unspecifically bound RNAP· σ^{54} complexes increased (data not shown).

Conformation of the closed complex of RNAP· σ^{54}

Another important piece of information that can be derived from the RNAP· σ^{54} -DNA images (Figures 1 and 2) is the relative position of the RNAP· σ^{54} to the DNA. Sometimes the protein seems to sit astride the DNA, whereas for other molecules the polymerase appears to be located on the side of the DNA fragment. We have distinguished nine conformations of specific RNAP· σ^{54} complexes at the promoter, and these are shown in Figure 4. The differences between these conformations were the direction of bending, the relative position of RNAP· σ^{54} to the DNA, and the side with which the polymerase was bound to the surface (see also Hansma *et al.*, 1998). For example, the complexes displayed in Figure 2a would be classified as 4h (left complex), 4d (middle complex) and 4e (right complex). The results from this type of analysis are summarized in Table 2. It has been reported that His-tagged RNAP· σ^{70} binds preferentially in the left-handed conformation (Figure 4d to f) to the mica surface (Hansma *et al.*, 1998). For the RNAP· σ^{54} holoenzyme studied here that was

Table 1. Percentage of complexes bound at different positions of the template

	Buffer (%)	Air (%) (1 ml wash)	Air (%) (50 ml wash)
Promoter	70	68	32
Other sites	17	21	38
Ends	13	11	30

A total of about 1800 complexes was evaluated. Only molecules that were not obstructed by other complexes and had only one RNAP· σ^{54} molecule bound were included in the analysis.

formed with His-tagged σ^{54} , a corresponding effect was not observed. The number of right-handed (Figure 4a to c) and left-handed (Figure 4d to f) conformations was approximately the same (Table 2), demonstrating that with our holo-enzyme preparation no side was preferred for binding to the surface. In buffer, about two-thirds of the RNAP· σ^{54} complexes were located at the side of the DNA template (lateral, Table 2) rather than sitting astride the DNA (centered, Table 2). The direction of the DNA bending at the promoter was in most cases away from the RNAP· σ^{54} , as in Figure 4b and e. The latter conformation is the one that was observed the most frequently.

DNA bending of the RNAP· σ^{54} -DNA complexes

A structural feature of RNAP· σ^{54} -DNA complexes that can be determined from the SFM images is the apparent DNA bending angle induced by binding of RNAP· σ^{54} . The distribution of bending angle measured for the different samples is displayed in Figure 5 and the mean values, 95% confidence intervals and standard deviations are summarized in Table 3. The distributions were fitted to the Gauss functions

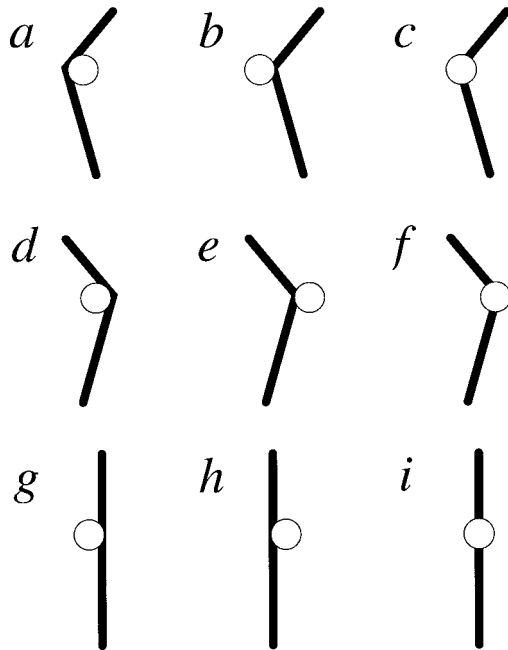


Figure 4. Observed conformations of the RNAP· σ^{54} closed complexes. Nine conformations for the specific RNAP· σ^{54} -DNA closed complexes could be distinguished on the images. The criteria for distinguishing between different conformations were the side with which the polymerase was bound to the surface (left-handed, right-handed, unknown), the position of the RNAP· σ^{54} relative to the DNA (centered or lateral), and the direction of the DNA bend (away from the RNAP· σ^{54} , around the RNAP· σ^{54} , unknown).

Table 2. Conformations of closed RNAP· σ^{54} -DNA complexes

	Buffer (%)	Air (%)
RNAP binding side ^a		
Right-handed (Fig. 4a–c)	40	47
Left-handed (Fig. 4d–f)	49	47
Unknown (Fig. 4g–i)	11	6
Position of RNAP relative to the DNA		
Centered (Fig. 4c, f, i)	36	43
Lateral (Fig. 4a, b, d, e, g, h)	64	57
Direction of bending		
Away from the RNAP (Fig. 4b, e)	41	47
Around the RNAP (Fig. 4a, d)	18	8
Unknown (Fig. 4c, f, g, h, i)	41	45

The Table shows the results of the measurements of the different conformations depicted in Figure 4. Only specific RNAP· σ^{54} -DNA complexes in fluid and air (1 ml wash) were analyzed. The absolute numbers for the nine conformations were: a 67, b 34, c 68, d 11, e 141, f 58, g 4, h 18, i 28 (buffer) and a 12, b 49, c 50, d 7, e 60, f 42, g 3, h 3, i 8 (air).

^a The conformations in Figure 4a to c and d to f are mirror images and can be assigned to complexes in the same conformation bound at opposite sides to the mica surface. See Hansma *et al.* (1998) for the designation as left-handed and right-handed complexes.

given below:

$$g(\theta) = A \exp\left(-\frac{(\theta - \bar{\theta})^2}{2 \cdot \sigma^2}\right) \quad (1)$$

In equations (1) and (2), $\bar{\theta}$ is the average DNA bending angle and σ the standard deviation. The distributions were truncated at a DNA bending angle of $\theta = 0$, because always the smallest angle θ was measured. We did not distinguish between left-handed (Figure 4d to f) and right-handed (Figure 4a to c) complexes, which would be equivalent to measuring the bending angle with both positive and negative values to account for the different directions of bending (Hansma *et al.*, 1998; Le Cam *et al.*, 1994). To account for this effect, we have also included a fit of the data in Figure 5 to a sum of two Gaussians that are centered around $\bar{\theta}$ and $-\bar{\theta}$:

$$g(\theta) = A \left[\exp\left(-\frac{(\theta - \bar{\theta})^2}{2 \cdot \sigma^2}\right) + \exp\left(-\frac{(\theta + \bar{\theta})^2}{2 \cdot \sigma^2}\right) \right] \quad (2)$$

If bending were isotropic, i.e. positive and negative values of $\bar{\theta}$ were equally probable, one would expect that the fit of the data to equation (2) would be better than that to equation (1). However, this is not the case, as can be seen from comparing the two fit curves in Figure 5. From the fit to a single Gaussian we determined a DNA bending angle (standard deviation) of $26(\pm 34)^\circ$ for the closed complex imaged in buffer and $32(\pm 45)^\circ$ in air. The distribution for the DNA bending angles of the unspecific complexes in fluid (Figure 5c) and in air (Figure 5d) was much broader than that for the specific complexes (Figure 5a and b). For the unspecific complexes in air, the data from both measurements in air (1 ml and 50 ml wash) were

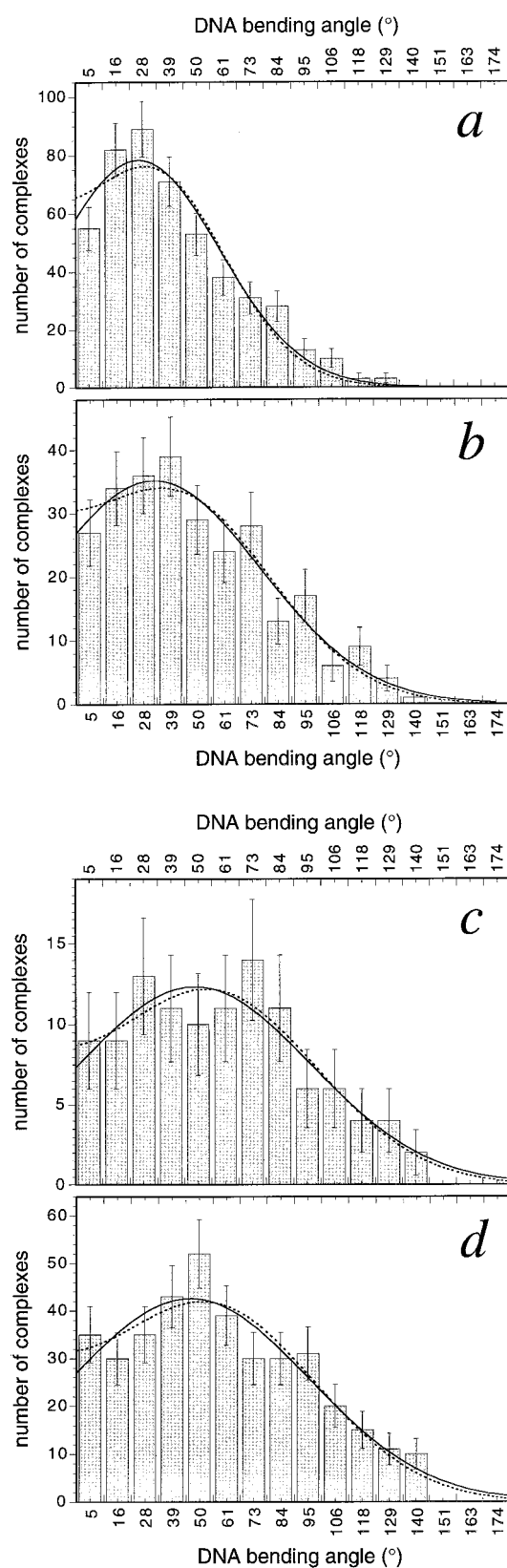


Figure 5. Histogram of the bending angles for RNAP· σ^{54} -DNA complexes. a, Histogram of the bending angles for specific RNAP· σ^{54} -DNA complexes in fluid. b, Histogram of the bending angles for specific RNAP· σ^{54} -DNA complexes in air. c, Histogram of the bending angles for unspecific RNAP· σ^{54} -DNA complexes in fluid. d, Histogram of the bending angles for

Table 3. Bending angles (degrees) of RNAP· σ^{54} -DNA complexes and free promoter DNA

	Buffer	Air
Specific complexes		
Mean \pm 95% confidence interval ^a	41 \pm 2	50 \pm 4
Mean \pm SD from Gaussian fit ^b	26 \pm 34	32 \pm 45
Complexes evaluated	476	267
Unspecific complexes		
Mean \pm 95% confidence interval	60 \pm 7	60 \pm 4
Mean \pm SD from Gaussian fit	49 \pm 48	46 \pm 49
Complexes evaluated	110	381
Free promoter DNA ^c		
Mean \pm 95% confidence interval	33 \pm 4	22 \pm 2
Mean \pm SD from Gaussian fit	0 \pm 44	0 \pm 27
Complexes evaluated	151	364

^a Mean value of all values \pm the 95% confidence interval of the mean.

^b Mean value determined from the Gaussian fit \pm the standard deviation of the mean.

^c The intrinsic bending of the promoter was measured with a circular mask (see Materials and Methods). DNA with NtrC bound at the enhancer was used to determine the location of the promoter.

pooled and analyzed together, since the two distributions were indistinguishable.

According to a Wilcoxon rank sum test, there was a significant difference between bending angles of the specific complexes in fluid and in air with a p value of 0.0011, whereas for the unspecific complexes no significant difference was detectable. The intrinsic bending of the promoter DNA was determined in the absence of RNAP· σ^{54} with a circular mask placed at the position of the promoter (see Materials and Methods). This mask had the same size as the apparent dimensions of the complex of RNAP· σ^{54} and the promoter DNA for which an average diameter of 35 nm in fluid or 27 nm in air was measured. The distribution obtained from these measurements is shown in Figure 6a and b. In both cases the Gaussian fit was excellent and was centered around 0°, as expected for an unbend DNA fragment, demonstrating that the *glnA* promoter had no intrinsic curvature.

DNA persistence length

As demonstrated by conventional EM (Théveny *et al.*, 1988), cryo-EM (Bednar *et al.*, 1995), and SFM (Hansma *et al.*, 1997; Rivetti *et al.*, 1996), the DNA persistence length can be determined from the conformation of single DNA molecules. The persistence length of the free DNA at the promoter was calculated from the observed average bending angle and 95% confidence intervals of 33(\pm 4)° (fluid) and 22(\pm 2)° (air) as described by Rippe *et al.* (1997a). Values of 65(\pm 10) nm and 52(\pm 29) nm

unspecific RNAP· σ^{54} -DNA complexes in air. The straight line refers to the Gaussian fit of a normal distribution (equation (1)), the broken line is a fit to equation (2).

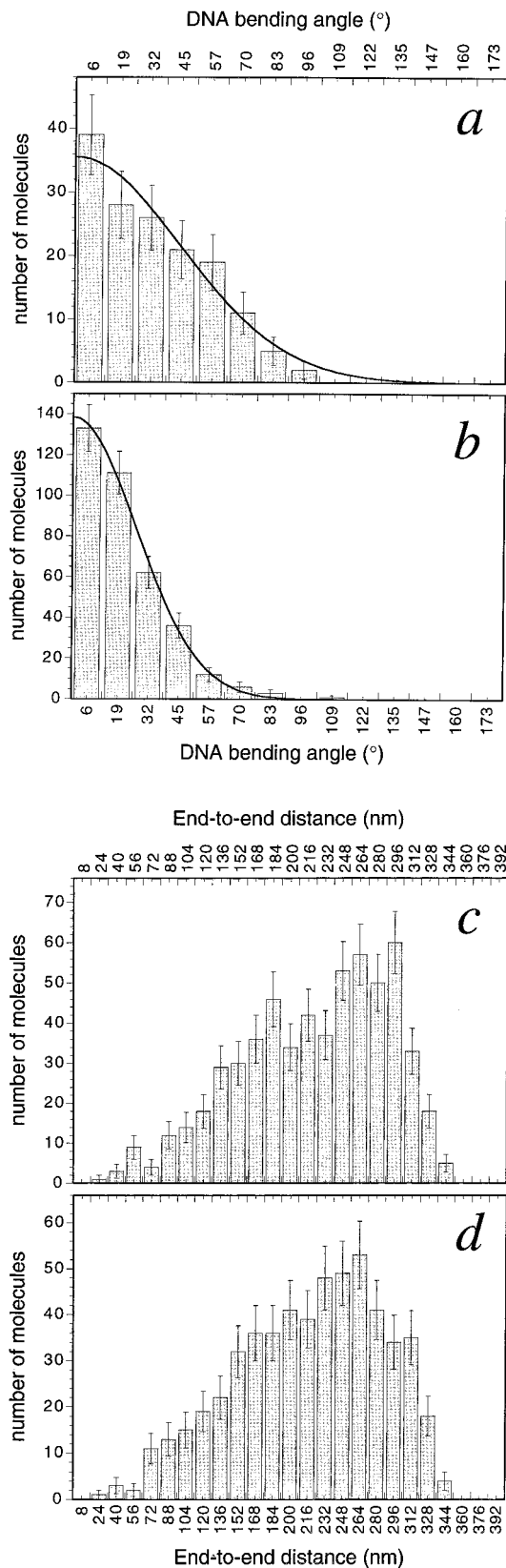


Figure 6. Histogram of the DNA bending angles at the *glnA* promoter and the distribution of DNA end-to-end distances. a, DNA bending angles at the *glnA* promoter in fluid observed in the absence of RNAP- σ^{54} . A mask with a diameter of 35 nm was positioned at the location of the promoter to mimic the dimensions of the

were obtained. Thus, within the relatively large error of the measurement, the DNA in this region did not appear to be significantly different in its flexibility from a random DNA sequence, which has a persistence length of about 50 nm (Hagerman, 1988).

In order to determine the average persistence length of the whole DNA fragment studied here, we measured the end-to-end distance of the free DNA. The left panels of Figure 6 show the distribution of the end-to-end distance in fluid (c) and in air (d). Using equation (9) from Rivetti *et al.* (1996) it is possible to calculate the persistence length from the measured average end-to-end distance of 222 nm in fluid and 218 nm in air in two dimensions. According to a Wilcoxon rank sum test, the distributions were not significantly different for the samples imaged in fluid and in air. The resulting average value of 47 nm for the persistence length is similar to the value obtained previously in air (Rivetti *et al.*, 1996) by SFM, where a persistence length of 53 nm was determined. Furthermore, our results indicate that no significant difference of the DNA flexibility is observed between samples imaged in buffer and in air for the protocols used. The DNA persistence length in solution has been determined by various methods to be around 50 nm (reviewed by Hagerman, 1988). Thus, our results support the conclusion made by Rivetti *et al.* (1996) that, for the protocols used here, the interactions between the DNA and the mica surface are relatively weak and do not preclude a re-equilibration of the DNA conformation on the surface.

DNA contour length

Another feature that can be determined from the SFM images is the apparent DNA contour length. The histograms for the different samples studied are displayed in Figure 7 (buffer) and in Figure 8 (air). The distributions for the contour length measurements in air were indistinguishable for the 1 ml and 50 ml wash. Accordingly, the data were pooled and analyzed together. The measurements of the apparent contour length yielded normal distributions to which a Gaussian fit and a *t*-test could be applied. The measured lengths for the free DNA (1036 bp) corresponded to a helical rise of $0.34(\pm 0.01)$ nm (fluid) and $0.33(\pm 0.01)$ nm (air). This is characteristic for B-DNA, which has a helical rise of 0.34 nm/base-pair, as determined by X-ray diffraction of DNA fibers (Leslie *et al.*, 1980). The distributions were broader for the protein-

RNA polymerase. b, DNA bending angles at the *glnA* promoter measured in air with a mask of 27 nm diameter. c and d, Histograms of the end-to-end distance distribution of the free DNA in fluid (c) and in air (d) from which the average DNA persistence length was determined.

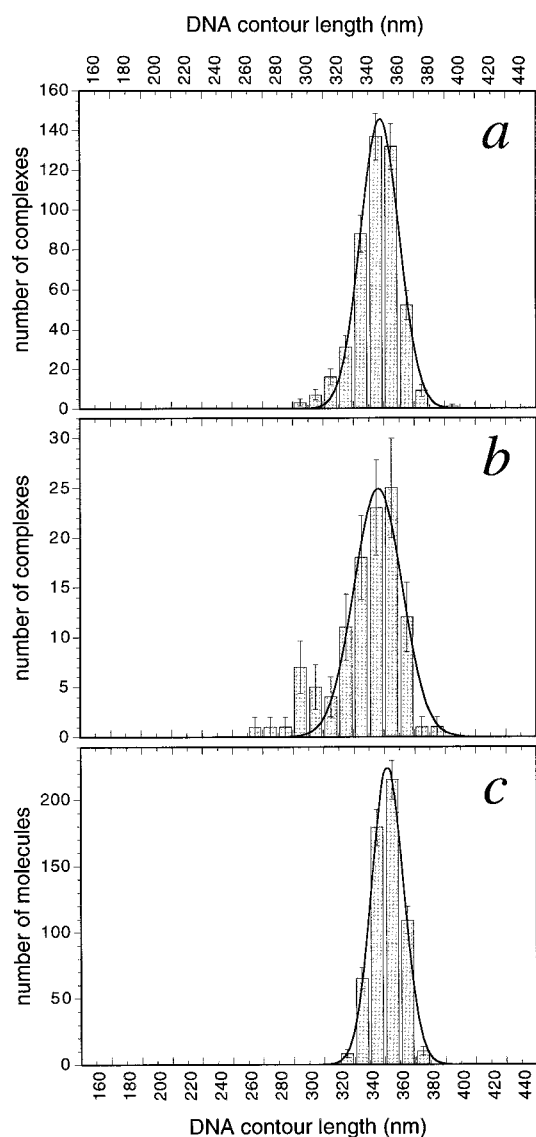


Figure 7. Histograms of the contour lengths measured in buffer. a, Specific RNAP· σ^{54} -DNA complexes. b, Unspecific RNAP· σ^{54} -DNA complexes. c, Free DNA.

DNA complexes that had standard deviations of 13 to 28 nm (Table 4) as compared to 11 nm for the free DNA. In fluid, mean values and 95% confidence intervals of 350(\pm 1) nm (specific complexes), 343(\pm 4) nm (unspecific complexes) and 356(\pm 1) nm (free DNA) were determined (Table 4). This showed that the binding of RNAP· σ^{54} at the promoter led to a relatively small but significant shortening of the DNA contour length by about 6 nm. In the unspecific complexes, this shortening was even more pronounced with a value of 13 nm. The results for the measurements in air are presented in Figure 8. For the free DNA (Figure 8c), the Gaussian fit had the same shape as for the free DNA in fluid (Figure 7c). The complexes imaged in air (Figure 8a and b) showed a broader distribution than those imaged in fluid. Apparent contour lengths of 320(\pm 2) nm for the specific, 310(\pm 3) nm

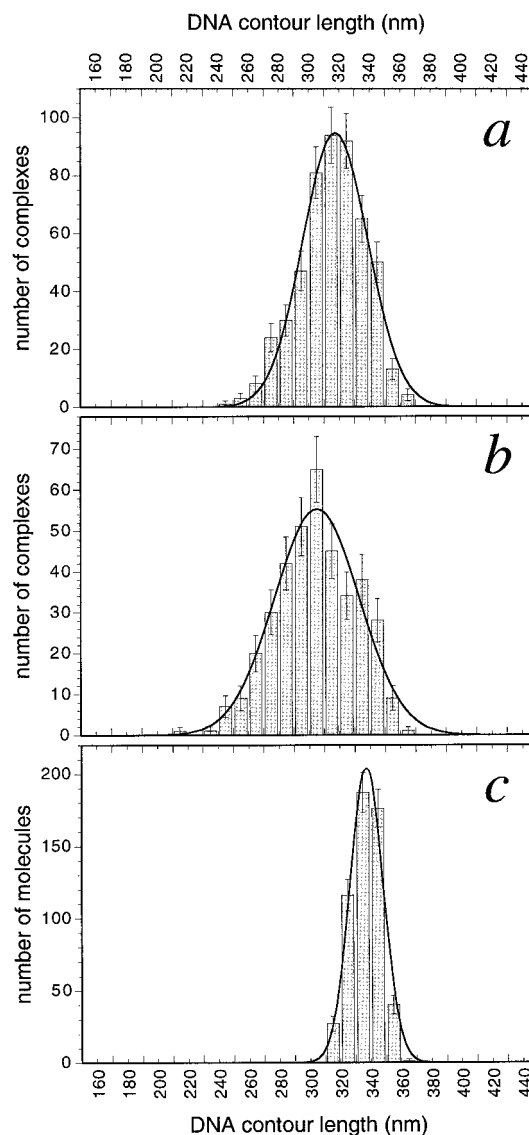


Figure 8. Histograms of the contour lengths measured in air. a, Specific RNAP· σ^{54} -DNA complexes. b, Unspecific RNAP· σ^{54} -DNA complexes. c, Free DNA.

for the unspecific complexes, and 342(\pm 1) nm for the free DNA were determined (Table 4). Thus, in air a very large decrease of the apparent DNA contour length of 22 and 32 nm for the protein-DNA complexes was observed as compared to the contour length of the free DNA.

Discussion

DNA-binding positions and bending angle of RNAP· σ^{54} imaged by SFM

Scanning force microscopy can be applied to study protein-DNA complexes in physiological buffers as done here for RNAP· σ^{54} and a template with the *glnA* promoter. The quality of the images obtained by using protocol I (Materials and Methods) was very good and comparable to those

Table 4. Apparent contour length (nm) of RNAP· σ^{54} -DNA complexes and free DNA

	Buffer	Air
Specific complexes		
Mean \pm 95% confidence interval ^a	350 \pm 1	320 \pm 2
Mean \pm SD from Gaussian fit ^b	353 \pm 13	323 \pm 21
Complexes evaluated	476	512
Unspecific complexes		
Mean \pm 95% confidence interval	343 \pm 4	310 \pm 3
Mean \pm SD from Gaussian fit	351 \pm 16	310 \pm 28
Complexes evaluated	110	381
Free DNA		
Mean \pm 95% confidence interval	356 \pm 1	342 \pm 1
Mean \pm SD from Gaussian fit	357 \pm 11	342 \pm 11
Helical rise per base-pair (nm)	0.34 \pm 0.01	0.33 \pm 0.01
Complexes evaluated	586	547

^a Mean value of all values \pm the 95% confidence interval of the mean.

^b Mean value determined from the Gaussian fit \pm the standard deviation of the mean.

acquired in air. Thus, it was possible to analyze the conformation of the molecules as described above and to compare the effect of different sample preparations.

The binding of the complexes to the surface is predominantly mediated by the DNA. Freshly cleaved mica is negatively charged and Mg²⁺ can promote electrostatic interactions between the mica surface and the negatively charged phosphate groups of the DNA (Bezanilla *et al.*, 1995; Bustamante & Rivetti, 1996). Other divalent cations like Ni²⁺ used here in protocol I or Co²⁺, and Zn²⁺ can replace Mg²⁺ and bind the DNA more tightly to the mica (Hansma & Laney, 1996). The presence of additional monovalent ions decreases the binding affinity of the DNA to the mica surface, probably by competition with the divalent cations (Bezanilla *et al.*, 1995). The RNAP· σ^{54} holoenzyme could bind to the mica also in the absence of DNA, albeit less efficiently (data not shown). This interaction is presumably also due to electrostatic interactions between charged amino acid residues and the mica surface, as it has been suggested for lysozyme (Radmacher *et al.*, 1994). However, since the charge density of the protein is much lower than that of the DNA, one would expect that the protein binds less tightly to the surface.

Millimolar concentrations of Ni²⁺, which are used in protocol I, or Zn²⁺ inhibit the transcription activity of RNA polymerase by competing with the magnesium ion that is required in the catalytic site for the formation of the new phosphodiester bond (Erie *et al.*, 1992; Niyogi & Feldman, 1981). However, it has been shown that RNAP-DNA complexes can be bound to mica in the presence of 2 mM Zn²⁺ and remain in a transcription-competent state (Kasas *et al.*, 1997). If the Zn²⁺ was washed away, the transcription activity was restored. For the samples prepared according to protocol I, complex formation of RNAP· σ^{54} and DNA, and the initial binding to the mica surface were conducted in 5 mM Hepes-KOH (pH 8.0),

10 mM magnesium-acetate, 50 mM potassium-acetate buffer, in which RNAP· σ^{54} is transcriptionally active. The addition of Ni²⁺ was solely required to attach the DNA more strongly to the surface and thereby significantly improving the image quality (Hansma & Laney, 1996). Thus, it appears unlikely that Ni²⁺ induces a conformation of the complexes that is different from that observed with only Mg²⁺ in the buffer although it reversibly inhibits transcription.

The SFM experiments were conducted under conditions where the open complex of RNAP· σ^{54} cannot be formed. Accordingly, only the closed complex of RNAP· σ^{54} bound specifically at the *glnA* promoter and RNAP· σ^{54} bound unspecifically at other sites of the template were present in the samples. For RNAP· σ^{70} it has been shown previously that the holoenzyme does not only bind specifically to the promoter sequence but also unspecifically to other sites of the DNA (deHaseth *et al.*, 1978). Relatively tight binding of the enzyme to non-initiating sites as well as binding to the ends has been reported (Melancon *et al.*, 1982, 1983). The various modes of binding of *E. coli* RNA polymerase have been observed here directly for the RNAP· σ^{54} holoenzyme. The analysis of the binding positions of RNAP· σ^{54} indicated that under appropriate conditions about 70% of the complexes were bound specifically at the promoter. Upon extensive washing of the samples, the enzyme can be moved by an external flow from the promoter to other positions of the template. This observation supports the view that RNA polymerase can slide along the DNA template. Sliding has been monitored directly by SFM for *E. coli* core RNA polymerase (Bustamante *et al.*, 1997) and for rhodamine-labeled RNAP· σ^{70} holoenzyme by fluorescence imaging (Kabata *et al.*, 1993). In addition, it has been concluded on the basis of kinetic measurements (Singer & Wu, 1987, 1988) and analysis of the promoter occupancy of different templates (Ricchetti *et al.*, 1988) that RNAP· σ^{70} is able to slide along the DNA. An alternative explanation for the observed dislocation of the protein during the washing step would be the dissociation and rebinding of the polymerase. However, we believe that the probability of such an event is very small and that the observed changes in the binding position (Figure 3) reflect sliding of the RNA polymerase. Washing the mica surface with water as done in protocols II and III effectively removes all molecules that are not bound to the surface. This is demonstrated by the experiments reported by Rivetti *et al.* (1996), where the kinetics of DNA-binding to the mica surface were studied by washing at different times after depositing the sample to the surface. The results show that the binding process is solely diffusion-controlled. A DNA diffusion coefficient of $D = 5.5 \times 10^{-8}$ cm²/second was determined in very good agreement with a theoretical value of $D = 5.4 \times 10^{-8}$ cm²/second for the DNA studied. If a significant amount of DNA molecules would still bind during the washing step,

this would be inconsistent with the observed results. Thus, it appears unlikely that a dissociated RNA polymerase can rebind to the DNA while the sample is rinsed with water.

The average bending angle and standard deviation for the specific complexes imaged in buffer was slightly smaller with a value of $26(\pm 34)^\circ$ versus $32(\pm 45)^\circ$ in air (Table 3). No significant difference was detectable for the unspecific complexes that showed a broad distribution with an average bending angle around 60° indicative of the presence of multiple conformations (Figure 6, Table 3). This demonstrates that the procedure of rinsing and removing excess liquid from the mica surface after deposition had little influence on the DNA bending angle. However, the unspecific complexes had a higher average bending angle and washing the samples caused an increase of the relative amount of these species. This could potentially affect the values of the specific complexes, in as much as unspecific complexes were present in the binding-site region of $r = 0.40(\pm 0.06)$ that was assigned to the specific complexes. However, this effect should be small. It can be estimated from the baseline of the Gaussian fit in Figure 3 that the amount of unspecifically bound RNA polymerase included with the specific complexes ($r = 0.40(\pm 0.06)$) should be only about 11% in buffer (Figure 3a) and 15% in air (Figure 3b).

The separate analysis of the various complex conformations in which the DNA was bent (Figure 4a to f) revealed significant differences with respect to the magnitude of the bending angle. The following values were determined for the images obtained in buffer according to protocol I. For the complexes in which the DNA was wrapped around the polymerase (Figure 4a and d, $n = 78$) a mean bending angle (standard deviation) of $39(\pm 28)^\circ$ was determined. In contrast, when the DNA was pointing away from the polymerase (Figure 4b and e, $n = 175$), the corresponding value was $52(\pm 30)^\circ$, and for the centered polymerase (Figure 4c and f, $n = 126$) it was $45(\pm 28)^\circ$. The results for the complexes imaged in air were similar to those in fluid. Thus, the relative large standard deviation in the bending angle of the specific complexes can be explained, at least in part, by the coexistence of multiple species with somewhat different bending angles. However, for an accurate comparison of the different conformations, the database is yet too small. In addition, it remains to be studied to what extent the different conformations of the complexes detected on the SFM images reflect also different conformation states of the RNA polymerase free in solution or result from the deposition of a single uniform species at different orientations relative to the surface. For the contour length, no correlation between the complex conformation and the measured contour length was detected.

In a previous study of RNAP· σ^{54} closed complexes by SFM, a bending angle of $50(\pm 24)^\circ$ was determined in air (Rippe *et al.*, 1997a), in contrast

to the value of $32(\pm 45)^\circ$ that was measured here for the samples prepared according to protocol II. Several differences are apparent when comparing the experimental conditions; namely, the lower salt concentration and the length of the DNA fragment, which was only 726 bp in the previous study. In addition, the deposition of the samples according to protocols II and III has been done in the presence of 0.01% NP-40, which was found to lead to more reproducible images. The effect of NP-40 on the bending angle of the complexes imaged in air was not studied systematically. It is possible that some of the observed differences in the bending angle distribution to the previous study reflect an influence of NP-40 (Rippe *et al.*, 1997a). However, this appears not very likely, because the images acquired in buffer (no NP-40, protocol I) and in air with deposition in the presence of NP-40 (1 ml wash, protocol II) showed a very similar distribution of bending angles. Thus, at this point it is unclear if the relatively minor differences in the experimental conditions are responsible for a significant change in the apparent DNA bending angle measured in air by SFM.

DNA contour length measurements of the RNAP· σ^{54} -DNA complexes

Based on kinetic, thermodynamic, and footprinting studies for *E. coli* RNAP· σ^{70} , the scheme given in equation (3) has been derived for the transcription initiation process (reviewed by Polyakov *et al.*, 1995).



R is the RNAP· σ^{70} holoenzyme, P is the promoter DNA, RP_{c1} is the initial closed complex observed at temperatures $< 8^\circ\text{C}$, RP_{c2} (also designated as RP_i) is an intermediate complex observed between 8 and 21°C , and RP_o is the final open complex that forms above 25°C and in which the promoter DNA sequence is partly melted. The different RNAP· σ^{70} -DNA conformations have been studied by DNase I and hydroxyl radical footprinting (e.g. see Cowing *et al.*, 1989; Schickor *et al.*, 1990). In the hydroxyl radical footprinting experiments (Schickor *et al.*, 1990), an interaction between the RNAP· σ^{70} holoenzyme and the T7 A1 promoter was determined that extended from about positions -53 to -4 (≈ 17 nm) for RP_{c1} and from -53 to $+21$ (≈ 25 nm) for RP_{c2} . The RP_o complex showed also a protection from -53 to $+21$, like the RP_{c2} form, but in addition the DNA was melted in the region from about -7 to $+2$. Thus, the RNAP· σ^{70} holoenzyme covers the same extended region of the DNA in the RP_{c2} and RP_o complex. The closed complex of RNAP· σ^{54} appears to be functionally equivalent to the RP_{c1} conformation. Footprinting of the RNAP· σ^{54} closed complex at the *glnA* promoter shows a protection in the region from about -34 close to

the transcription start site at position -2 (≈ 10 nm). In the open complex, which should correspond to the RP_o form, the protected region is extended further to $+23$, i.e. to a region of about 19 nm of DNA (Popham *et al.*, 1989; Tintut *et al.*, 1994). The comparison of the footprinting patterns of the two holoenzyme forms reveals that with RNAP· σ^{54} the upstream contacts in the region from positions -53 to -35 are missing, which leads to a significantly shorter interaction region over only 10 nm *versus* 17 nm of promoter DNA.

The dimensions of the RNAP· σ^{70} holoenzyme have been determined by electron diffraction of two-dimensional crystals to be 10 nm \times 10 nm \times 16 nm (Darst *et al.*, 1989). Based on these data, it has been concluded that bending of the DNA would be necessary for RNA polymerase to interact with the 74 bp or 25 nm of DNA in the RP_{c2} and RP_o complex (Darst *et al.*, 1989). However, it should be noted that a somewhat more extended conformation of a heparin-stable RNAP· σ^{70} promoter complex (probably the RP_o form) with a maximum extension of the polymerase of $25(\pm 2)$ nm has been derived by small-angle neutron scattering studies (Heumann *et al.*, 1988). For RNAP· σ^{54} , an increase of the DNA bending angle was observed on SFM images acquired in air for the open complex as compared to the closed complex, which would be consistent with wrapping of the DNA around the polymerase in the open complex (Rippe *et al.*, 1997a). This increase of the DNA bending angle was accompanied by a reduction of the apparent contour length by 17 nm, supporting the interpretation that in the open complex of RNAP· σ^{54} the DNA wraps around the polymerase. A similar argument has been made for eukaryotic RNA polymerase II (Forget *et al.*, 1997; Kim *et al.*, 1997). In the two latter studies, an apparent reduction of the contour length by 50 and 51 base-pairs, or 17 nm, as compared to the free DNA was measured by conventional electron microscopy of ethanol-washed and air-dried samples. The experiments were made with a so-called preinitiation complex that is competent for transcription initiation but the DNA at the promoter has not been melted. This form of RNA polymerase II appears to be functionally equivalent to the intermediate RP_{c2} complex (Kim *et al.*, 1997).

Here we have analyzed only the closed complex of RNAP· σ^{54} at the *glnA* promoter and thus the results cannot be compared directly to intermediate or open RNA polymerase complexes. However, we would like to note that according to the present data, the large reduction of the apparent contour length observed with the samples imaged in air appears to be, at least partly, an artefact of drying the sample. The closed complexes imaged in buffer displayed a reduction by only 6 nm as compared to the free DNA, in contrast to a value of 22 nm measured in air (Table 4). It is difficult to conceive how over a protein-DNA contact region of ≈ 10 nm, as

determined from the footprint of RNAP· σ^{54} , the apparent DNA contour length could be reduced by 22 nm. Even if we would attribute the 6 nm reduction observed in buffer completely to the way imaging and contour length measurements were made, this would still leave 16 nm of DNA that are wrapped up in the RNAP· σ^{54} complex and, accordingly, should show protection in footprinting experiments, which is in contrast to the observed protection of only ≈ 10 nm. The logical conclusion is that upon drying the closed complex of RNAP· σ^{54} adopts an artificial conformation that has an increased interaction surface as compared to the native hydrated state. The observation that the unspecific complexes imaged in buffer showed a larger reduction by 13 nm indicates that the RNA polymerase can adopt multiple conformations that are different in the interaction with the DNA. The unspecific complex cannot be studied by footprinting techniques, since *per definitionem* it consists of an ensemble of species bound at different positions on the DNA. The results of our contour length measurements and the observed increase of the average DNA bending angle to $60(\pm 7)^\circ$ raise the possibility that the unspecifically bound RNAP· σ^{54} has an extended interaction surface similar to that of the open complex or the RP_{c2} of RNAP· σ^{70} .

Model for the closed complex of RNAP· σ^{54}

Approximately 850 specific closed complexes of RNAP· σ^{54} at the *glnA* promoter have been analyzed here by SFM, including about 400 molecules that were imaged in buffer. For these, the protein and DNA were kept in their native hydration state throughout the preparation. Thus, it appears reasonable to assume that the characteristic features of the native conformation of the RNAP· σ^{54} closed complex were better preserved than with previous SFM or EM imaging protocols that included washing and drying the sample. From the analysis of the RNAP· σ^{54} -DNA complexes, the following results were obtained. (i) In two-thirds of the complexes the RNA polymerase holoenzyme was located on the side of the DNA fragment. (ii) The maximum of the distribution of bending angles was at about 30° . (iii) For 70% of the complexes with a DNA bend, the direction of bending was away from the polymerase and only in 30% of the complexes the DNA was bent around the protein. (iv) The reduction of the apparent contour length by 6 nm as compared to the free DNA was relatively small.

Upon binding to the surface, the three-dimensional conformation of the complexes is constrained to two dimensions, and information on the orientation of the molecule in the third dimension is lost. In addition, the resulting images reflect different modes of binding the complex to the surface. Accordingly, even if the RNAP· σ^{54} closed complex was present in a single conformation free

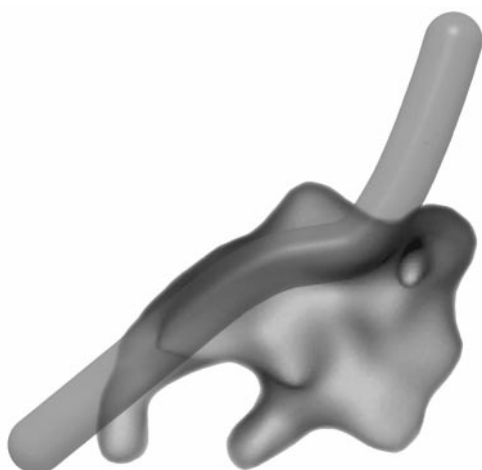


Figure 9. Model for the closed complex of RNAP· σ^{54} . A trajectory of the promoter DNA is shown that would be consistent with the results from the SFM image analysis in buffer as described in the text. For the structure of the RNA polymerase holoenzyme, the structure of *E. coli* RNAP· σ^{70} was adapted from Figure 5c of Polyakov *et al.* (1995). The irregularly shaped holoenzyme molecule is approximately 10 nm × 10 nm × 16 nm. The DNA is drawn as a transparent tube. The indicated interaction of the DNA with the RNA polymerase from the top down to the extrusion at the upper part of the finger-like structure would be in agreement with a protection of about ≈ 10 nm of DNA, as determined in footprinting experiments (Popham *et al.*, 1989; Tintut *et al.*, 1994).

in solution, one would obtain different two-dimensional images for the various asymmetric features of the structure that can be resolved by SFM. Thus, it is not surprising that the SFM images display an ensemble of distinctive conformations as depicted in Figure 4. In Figure 9 a model is presented for the trajectory of the DNA in the closed complex of RNAP· σ^{54} that would be consistent with the structural features that were observed most frequently on the SFM images. These were the lateral location of the polymerase with respect to the DNA, with only a moderate DNA bending angle of around 30° pointing away from the protein. In addition, the relatively small contour length reduction of 6 nm indicated that the DNA was not wrapped around the polymerase. If the DNA was wrapped around the polymerase completely, one would expect a much larger apparent shortening of the apparent DNA contour length by 20 to 30 nm. In addition, this is likely to require a much more extended protein-DNA contact region than the 10 nm or 32 bp measured by footprinting of RNAP· σ^{54} closed complex (Popham *et al.*, 1989; Tintut *et al.*, 1994). The RNA polymerase structure shown in Figure 9 is that of the *E. coli* RNAP· σ^{70} holoenzyme determined previously by electron microscopy of negatively stained, two-dimensional crystals at ≈ 28 Å resolution (Darst *et al.*, 1989). Obviously, we have no information on the

exact path of the DNA, and the structures of RNAP· σ^{54} and RNAP· σ^{70} might be different. The model has been made with the intention to demonstrate how the results from our SFM experiments could be accommodated with a structure of the RNAP· σ^{70} holoenzyme. Models for the trajectory of the DNA in the closed complex of RNAP· σ^{70} in the RP_{c1} and RP_{c2} conformation have been proposed that imply wrapping of the DNA around the holoenzyme (e.g. see Figure 6 of Polyakov *et al.*, 1995). This view is based mostly on topological studies of *E. coli* RNAP· σ^{70} and the wild-type and L8UV5 lactose promoters in which a topological unwinding of 1.3 to 1.7 turns was observed in the absence of a detectable amount of strand separation. Accordingly, the observed unwinding has been assigned to the formation of a closed complex form in which the DNA is wrapped around the polymerase (Amouyal & Buc, 1987). It should be noted that these experiments were conducted at 37°C and it is difficult to assess whether the RNA polymerase conformation with the unmelted promoter DNA refers to the RP_{c1} or the RP_{c2} complex or a mixture of both. Since both forms have a very different footprinting pattern, as discussed above, this is a crucial point for the interpretation of the data. While several lines of evidence support the view that the DNA is at least partly wrapped around the polymerase in the RP_{c2} and RP_o conformation, this might be different for the RP_{c1} form. With respect to the maximal extension of 16 nm (Darst *et al.*, 1989) or $25(\pm 2)$ nm (Heumann *et al.*, 1988) determined for RNAP· σ^{70} and the footprint of 17 nm, it appears possible that there is little or no wrapping of the DNA in the RP_{c1} conformation. For the RNAP· σ^{54} closed complex, the footprint covers only 10 nm of promoter DNA and, on the basis of the results presented here, we expect the major features of the structure of the RNAP· σ^{54} closed complex to resemble the model displayed in Figure 9.

Materials and Methods

Preparation of protein and DNA samples

Expression and purification of His-tagged σ^{54} protein from pS54-2 was done as described (Rippe *et al.*, 1997a). RNA polymerase core enzyme from *E. coli*, which was a kind gift of Hermann Heumann, MPI München, was mixed with σ^{54} in a ratio of 1:2.5 to form the RNA polymerase holoenzyme at a stock concentration of ≈ 1 μM . The activity of this holoenzyme preparation was confirmed in *in vitro* transcription experiments as described (Rippe *et al.*, 1998). The DNA fragment used for the protein binding was the 1036 bp linear *PvuII-PvuII* from pJES534 (Klose *et al.*, 1993). In this template, the *glnA* promoter is positioned 139 nm (410 bp) from one end of the fragment and 213 nm (626 bp) away from the other end, where two NtrC binding sites are located. The fragment was purified by HPLC chromatography (buffer A, 50 mM Tris-HCl (pH 7.5), 0.2 M NaCl, 0.1 mM EDTA; buffer B, 50 mM Tris-HCl (pH 7.5), 0.8 M NaCl, 0.1 mM

EDTA) using the Gen-PakTM Fax resin from Millipore (Milford, MA). The flow-rate was 0.5 ml min⁻¹ and a gradient from 0.44 M to 0.50 M NaCl in 2.5 ml, 0.50 M to 0.53 M NaCl in 2.5 ml, 0.53 M to 0.55 M NaCl in 15 ml, and 0.55 M to 0.57 M NaCl in 10 ml was used to elute the DNA. The peak of the eluted DNA was desalted on a NAP-5 column (Pharmacia, Germany) and stored in 10 mM Tris-HCl (pH 7.5), 10 mM NaCl, 0.1 mM EDTA. DNA fragment concentrations were determined by absorbance measurements using an extinction coefficient of 6500 M⁻¹ cm⁻¹ per nucleotide at 260 nm. Protein-DNA complexes were formed by incubating RNAP· σ^{54} and the DNA template at the indicated concentrations for ten minutes at 37°C in 5 mM Hepes-KOH (pH 8.0), 10 mM magnesium-acetate, 50 mM potassium-acetate (=0.5 × HS buffer). The ratio of RNAP· σ^{54} to the DNA template ranged from 0.8:1 to 1.0:1.0.

From titrations of the RNAP· σ^{54} concentration in *in vitro* transcription experiments (Rippe *et al.*, 1998), we estimate that the transcription activity of our holoenzyme preparation was of the order of 40 to 70% with respect to the concentration of RNA polymerase core enzyme. An accurate determination of the activity for RNAP· σ^{54} is more difficult than with RNAP· σ^{70} , since transcription by RNAP· σ^{54} requires the formation of a phosphorylated NtrC octamer at the enhancer that interacts with the polymerase at the promoter. The activity of RNAP· σ^{54} with respect to specific DNA binding was >70% as estimated from the SFM work. The experiments conducted at a RNAP· σ^{54} /DNA template ratio of 1:1 showed an almost complete saturation of the DNA with polymerase if protocols I and II were used (Figure 1a and b). Thus, the general DNA-binding activity of our RNAP· σ^{54} protein preparation was >90%.

Scanning force microscopy

The SFM images were obtained with a Nanoscope III (Digital Instruments, Santa Barbara, CA) operating in the tapping mode, where the cantilever is oscillated vertically while it is scanned over the surface. The three different protocols described below were used:

Protocol I (buffer)

For imaging in buffer, the SFM fluid cell (Digital Instruments) was mounted onto a freshly cleaved mica disc (Plano GmbH, Wetzlar, Germany). With this setup, an O-ring seals the cell with the sample surface so that the liquid is confined to a volume of about 30 μ l. The cell was filled with a solution of RNAP· σ^{54} and the DNA fragment in 0.5 × HS buffer at a concentration of 0.5 to 1 nM RNAP· σ^{54} -DNA complexes. Then the sample was allowed to equilibrate for ten minutes. At this stage the complexes were barely visible, most likely because they did not adhere very well to the surface and were able to move as observed previously (e.g. see Rippe *et al.*, 1997b,c). To bind the DNA more tightly to the mica surface, 60 μ l of a solution containing 5 mM Hepes-KOH (pH 8.0), 2 mM MgCl₂ and 5 mM NiSO₄ was injected. After addition of the Ni²⁺-containing buffer, the complexes remained stably bound to the surface and good images could be obtained reproducibly. It was possible to change the solution in the fluid cell back to 0.5 × HS buffer without any apparent effect on the con-

formation of the complexes, except that flushing the fluid cell with high flow-rates reduced the number of specific complexes, as discussed above. Images were acquired in the tapping mode using sharpened electron beam deposited tips from Nanotools, München, Germany. The tips were made of silicon with a typical force constant of 1 to 5 N/m, a resonance frequency in air around 70 to 90 kHz, and a tip curvature radius of 5 to 10 nm (specifications as given by the manufacturer). For scanning in buffer, vibration frequencies between 18 and 30 kHz were used.

Protocol II (air, 1 ml wash)

Protein-DNA complexes were formed by incubating 3 to 4 nM 1036 bp *PvuII* fragment from pJES534 with 3 nM RNAP· σ^{54} in 0.5 × HS buffer for ten minutes at 37°C. After incubation, 0.2% (v/v) Nonidet-P 40 was added to a final concentration of 0.01% and 20 μ l of the mix were deposited onto a freshly cleaved mica. The mica disc was washed right away by dropping distilled water (1 ml) onto the surface and then drying the sample in a stream of N₂. Images were recorded in air at ambient humidity using etched Si-probes (type Nanosensors) purchased from L.O.T. Oriel (Darmstadt, Germany) with a force constant of 17 to 64 N/m, a thickness of 3.5 to 5.0 μ m, a resonance frequency between 250 and 400 kHz, and a tip curvature radius of \approx 10 nm (specifications as given by the manufacturer).

Protocol III (air, 50 ml wash)

The samples were prepared as described for protocol II, but with concentrations of 4 to 10 nM RNAP· σ^{54} and 1 to 2 nM DNA. After deposition of the sample onto the mica disk, it was washed with 50 ml of distilled water. Further processing and imaging were as described for protocol II.

Image analysis

Only molecules with a single RNAP· σ^{54} holoenzyme bound to the DNA fragment were analyzed that were not obstructed by other DNA fragments or protein molecules. Complexes with the protein being bound at the end of the DNA were not included into the analysis, except for the data given in Table 1. Measurements of the DNA bending angle and the DNA contour length were done with the program NIH image v. 1.58 (National Institutes of Health, Bethesda, MD). The data were plotted and fitted with the program Kaleidagraph (Synergy Software, PA). The error bars for each bin correspond to the square-root of the number of samples within each bin. At least five independent experiments were analyzed for the complexes studied in fluid and in air. Statistical analysis of the data was performed with the program JMP version 3.1.5 (SAS Institute Inc.). A *t*-test was used to compare whether the mean values for the Gaussian-shaped distributions in Figures 3, 6a, 6b, 7 and 8 were different, whereas the asymmetric distribution in Figures 5, 6c and 6d were analyzed with a Wilcoxon rank sum test.

Analysis of the RNAP· σ^{54} binding sites

The length of the DNA from the center of the bound RNA polymerase to the two ends of the DNA was determined. Then the ratio r of the length of the short arm to the total contour length was calculated. The *glnA* promoter is located 139 nm away from one end of the DNA and 213 nm from the other end with a total contour length of 352 nm. This corresponds to a theoretical value of $r = 0.04$ for the closed complex of RNAP· σ^{54} at the promoter. The histogram of the measured values of r showed a Gaussian distribution centered around the expected position of the promoter. Complexes that were within two standard deviations of the position of the promoter were classified as specific closed complexes and those that were outside this range were designated as unspecifically bound RNA polymerase.

Measurement of DNA bending angles

The DNA bending angles of DNA-bound RNAP· σ^{54} were measured with the NIH image Software by drawing lines through the DNA axes on both sides of the polymerase and measuring the angle α at their intersection (Rees *et al.*, 1993). The DNA bending angle θ is then defined as $\theta = 180^\circ - \alpha$. The intrinsic bending of the *glnA* promoter region of free DNA were determined by using DNA fragments with NtrC^{D54E,S160F} bound at the enhancer for dried samples or wild-type NtrC bound to the enhancer for probes in fluid. Then a circular mask with the apparent dimensions of the RNA polymerase (27 nm diameter for dried samples, 35 nm for molecules in fluid) was placed at the position of the promoter and the DNA bending angle was determined. The distributions of DNA bending angles obtained were categorized into a number of bins that approximated the square-root of the number of samples over the range of values observed.

Measurements of apparent contour length

The same complexes for which DNA bending angles were determined were used for measurements of the apparent DNA contour length. In addition, 586 free DNA molecules in fluid and 547 free DNA molecules in air were analyzed. The contour length was determined by drawing a curved line through the middle of the DNA contour, starting from one end of the molecule to the other end. For the protein-DNA complexes, the curve was drawn through the center of the protein from the DNA entry and exit points.

Acknowledgments

We thank Nathalie Brun for help with the HPLC purification of the DNA and Hermann Heumann for *E. coli* RNA polymerase core enzyme. This work was supported by DFG grant Ri 828/1.

References

Amouyal, M. & Buc, H. (1987). Topological unwinding of strong and weak promoters by RNA polymerase. A comparison between the lac wild-type and the UV5 sites of *Escherichia coli*. *J. Mol. Biol.* **195**, 795–808.

- Bednar, J., Furrer, P., Katritch, V., Stasiak, A. Z., Dubochet, J. & Stasiak, A. (1995). Determination of DNA persistence length by cryo-electron microscopy. Separation of the static and dynamic contributions to the apparent persistence length of DNA. *J. Mol. Biol.* **254**, 579–594.
- Bezanilla, M., Manne, S., Laney, D. E., Lyubchenko, Y. L. & Hansma, H. G. (1995). Adsorption of DNA to mica, silylated mica, and minerals: characterization by atomic force microscopy. *Langmuir*, **11**, 655–659.
- Bustamante, C. & Rivetti, C. (1996). Visualizing protein-nucleic acid interactions on a large scale with the scanning force microscope. *Annu. Rev. Biophys. Biomol. Struct.* **25**, 395–429.
- Bustamante, C., Rivetti, C. & Keller, D. J. (1997). Scanning force microscopy under aqueous solutions. *Curr. Opin. Struct. Biol.* **7**, 709–716.
- Collado-Vides, J., Magasanik, B. & Gralla, J. D. (1991). Control site location and transcriptional regulation in *Escherichia coli*. *Microbiol. Rev.* **55**, 371–394.
- Cowing, D. W., Meccas, J., Record, M. T., Jr & Gross, C. A. (1989). Intermediates in the formation of the open complex by RNA polymerase holoenzyme containing the sigma factor sigma 32 at the groE promoter. *J. Mol. Biol.* **210**, 521–530.
- Darst, S. A., Kubalek, E. W. & Kornberg, R. D. (1989). Three-dimensional structure of *Escherichia coli* RNA polymerase holoenzyme determined by electron microscopy. *Nature*, **340**, 730–732.
- deHaseh, P. L., Lohman, T. M., Burgess, R. R. & Record, M. T., Jr (1978). Nonspecific interactions of *Escherichia coli* RNA polymerase with native and denatured DNA: differences in the binding behavior of core and holoenzyme. *Biochemistry*, **17**, 1612–1622.
- Erie, D. A., Yager, T. D. & von Hippel, P. H. (1992). The single-nucleotide addition cycle in transcription: a biophysical and biochemical perspective. *Annu. Rev. Biophys. Biomol. Struct.* **21**, 379–415.
- Forget, D., Robert, F., Grondin, G., Burton, Z. F., Greenblatt, J. & Coulombe, B. (1997). RAP74 induces promoter contacts by RNA polymerase II upstream and downstream of a DNA bend centered on the TATA box. *Proc. Natl Acad. Sci. USA*, **94**, 7150–7155.
- Guthold, M., Bezanilla, M., Erie, D. A., Jenkins, B., Hansma, H. G. & Bustamante, C. (1994). Following the assembly of RNA-polymerase-DNA complexes in aqueous solutions with the scanning force microscope. *Proc. Natl Acad. Sci. USA*, **91**, 12927–12931.
- Hagerman, P. J. (1988). Flexibility of DNA. *Annu. Rev. Biophys. Biomol. Struct.* **17**, 265–286.
- Hansma, H. G. & Hoh, J. H. (1994). Biomolecular imaging with the atomic force microscope. *Annu. Rev. Biophys. Biomol. Struct.* **23**, 115–139.
- Hansma, H. G. & Laney, D. E. (1996). DNA binding to mica correlates with cationic radius: assay by atomic force microscopy. *Biophys. J.* **70**, 1933–1939.
- Hansma, H. G., Kim, K. J., Laney, D. E., Garcia, R. A., Argaman, M., Allen, M. J. & Parsons, S. M. (1997). Properties of biomolecules measured from atomic force microscope images: a review. *J. Struct. Biol.* **119**, 99–108.
- Hansma, H. G., Bezanilla, M., Nudler, E., Hansma, P. K., Hoh, J., Kashlev, M., Firouz, N. & Smith, B. (1998). Left-handed conformation of histidine-tagged RNA

- polymerase complexes imaged by atomic force microscopy. *Probe Microsc.* **1**, 117–125.
- Heumann, H., Lederer, H., Baer, G., May, R. P., Kjems, J. K. & Crespi, H. L. (1988). Spatial arrangement of DNA-dependent RNA polymerase of *Escherichia coli* and DNA in the specific complex. A neutron small angle scattering study. *J. Mol. Biol.* **201**, 115–125.
- Kabata, H., Kurosawa, O., Arai, I., Washizu, M., Margaron, S. A., Glass, R. E. & Shimamoto, N. (1993). Visualization of single molecules of RNA polymerase sliding along DNA. *Science*, **262**, 1561–1563.
- Kasas, S., Thomson, N. H., Smith, B. L., Hansma, H. G., Zhu, X., Guthold, M., Bustamante, C., Kool, E. T., Kashlev, M. & Hansma, P. K. (1997). *Escherichia coli* RNA polymerase activity observed using atomic force microscopy. *Biochemistry*, **36**, 461–468.
- Kim, T. K., Lagrange, T., Wang, Y. H., Griffith, J. D., Reinberg, D. & Ebricht, R. H. (1997). Trajectory of DNA in the RNA polymerase II transcription preinitiation complex. *Proc. Natl Acad. Sci. USA*, **94**, 12268–12273.
- Klose, K. E., Weiss, D. S. & Kustu, S. (1993). Glutamate at the site of phosphorylation of nitrogen-regulatory protein NTRC mimics aspartyl-phosphate and activates the protein. *J. Mol. Biol.* **232**, 67–78.
- Le Cam, E., Fack, F., Menissier-de Murcia, J., Cognet, J. A., Barbin, A., Sarantoglou, V., Révet, B., Delain, E. & de Murcia, G. (1994). Conformational analysis of a 139 base-pair DNA fragment containing a single-stranded break and its interaction with human poly(ADP-ribose) polymerase. *J. Mol. Biol.* **235**, 1062–1071.
- Leslie, A. G. W., Arnott, S., Chandrasekaran, R. & Ratliff, R. L. (1980). Polymorphism of DNA double helices. *J. Mol. Biol.* **143**, 49–72.
- Lyubchenko, Y. L., Jacobs, B. L., Lindsay, S. M. & Stasiak, A. (1995). Atomic force microscopy of nucleoprotein complexes. *Scanning Microsc.* **9**, 705–727.
- Melancon, P., Burgess, R. R. & Record, M. T., Jr. (1982). Nitrocellulose filter binding studies of the interactions of *Escherichia coli* RNA polymerase holoenzyme with deoxyribonucleic acid restriction fragments: evidence for multiple classes of non-promoter interactions, some of which display promoter-like properties. *Biochemistry*, **21**, 4318–4331.
- Melancon, P., Burgess, R. R. & Record, M. T., Jr (1983). Direct evidence for the preferential binding of *Escherichia coli* RNA polymerase holoenzyme to the ends of deoxyribonucleic acid restriction fragments. *Biochemistry*, **22**, 5169–5176.
- Niyogi, S. K. & Feldman, R. P. (1981). Effect of several metal ions on misincorporation during transcription. *Nucl. Acids Res.* **9**, 2615–2627.
- North, A. K., Klose, K. E., Stedman, K. M. & Kustu, S. (1993). Prokaryotic enhancer-binding proteins reflect eukaryote-like modularity: the puzzle of nitrogen regulatory protein C. *J. Bacteriol.* **175**, 4267–4273.
- Palecek, E., Vlk, D., Stankova, V., Brazda, V., Vojtesek, B., Hupp, T. R., Schaper, A. & Jovin, T. M. (1997). Tumor suppressor protein p53 binds preferentially to supercoiled DNA. *Oncogene*, **15**, 2201–2209.
- Polyakov, A., Severinova, E. & Darst, S. A. (1995). Three-dimensional structure of *E. coli* core RNA polymerase: promoter binding and elongation conformations of the enzyme. *Cell*, **83**, 365–373.
- Popham, D. L., Szeto, D., Keener, J. & Kustu, S. (1989). Function of a bacterial activator protein that binds to transcriptional enhancers. *Science*, **243**, 629–635.
- Radmacher, M., Fritz, M., Hansma, H. G. & Hansma, P. K. (1994). Direct observation of enzyme activity with the atomic force microscope. *Science*, **265**, 1577–1579.
- Rees, W. A., Keller, R. W., Vesenka, G. Y. & Bustamante, C. (1993). Evidence of DNA bending in transcription complexes imaged by scanning force microscopy. *Science*, **260**, 1646–1649.
- Reitzer, L. J. & Magasanik, B. (1986). Transcription of *glnA* in *E. coli* is stimulated by activator bound to sites far from the promoter. *Cell*, **45**, 785–792.
- Ricchetti, M., Metzger, W. & Heumann, H. (1988). One-dimensional diffusion of *Escherichia coli* DNA-dependent RNA polymerase: a mechanism to facilitate promoter location. *Proc. Natl Acad. Sci. USA*, **85**, 4610–4614.
- Rippe, K., Guthold, M., von Hippel, P. H. & Bustamante, C. (1997a). Transcriptional activation via DNA-looping: visualization of intermediates in the activation pathway of *E. coli* RNA polymerase· σ^{54} holoenzyme by scanning force microscopy. *J. Mol. Biol.* **270**, 125–138.
- Rippe, K., Mücke, N. & Langowski, J. (1997b). Molecules in motion: imaging DNA with the scanning force microscope in aqueous solutions. *Bioforum Int.* **1**, 42–44.
- Rippe, K., Mücke, N. & Langowski, J. (1997c). Superhelix dimensions of a 1868 base-pair plasmid determined by scanning force microscopy in air and in aqueous solution. *Nucl. Acids Res.* **25**, 1736–1744.
- Rippe, K., Mücke, N. & Schulz, A. (1998). Association states of *E. coli* NtrC protein determined by analytical ultracentrifugation. *J. Mol. Biol.* **278**, 915–933.
- Rivetti, C., Guthold, M. & Bustamante, C. (1996). Scanning force microscopy of DNA deposited onto mica: equilibration versus molecular kinetic trapping studied by statistical polymer chain analysis. *J. Mol. Biol.* **264**, 919–932.
- Schaper, A. & Jovin, T. M. (1996). Striving for atomic resolution in biomolecular topography: the scanning force microscope (SFM). *Bioessays*, **18**, 925–935.
- Schickor, P., Metzger, W., Werel, W., Lederer, H. & Heumann, H. (1990). Topography of intermediates in transcription initiation of *E. coli*. *EMBO J.* **9**, 2215–2220.
- Singer, P. & Wu, C. W. (1987). Promoter search by *Escherichia coli* RNA polymerase on a circular DNA template. *J. Biol. Chem.* **262**, 14178–14189.
- Singer, P. T. & Wu, C. W. (1988). Kinetics of promoter search by *Escherichia coli* RNA polymerase. Effects of monovalent and divalent cations and temperature. *J. Biol. Chem.* **263**, 4208–4214.
- Théveny, B., Coulaud, D., Le, Bret M. & Révet, B. (1988). DNA sequence and structure. In *Structure & Expression, DNA Bending and Curvature* (Olson, W. K., Sarma, M. H., Sarma, R. H. & Sundaralingam, M., eds), vol. 3, pp. 39–55, Adenine Press, Schenectady, NY.

- Tintut, Y., Wong, C., Jiang, Y., Hsieh, M. & Gralla, J. D. (1994). RNA polymerase binding using a strongly acidic hydrophobic-repeat region of σ^{54} . *Proc. Natl Acad. Sci. USA*, **91**, 2120–2124.
- Wyman, C., Rombel, I., North, A. K., Bustamante, C. & Kustu, S. (1997). Unusual oligomerization required for activity of a bacterial enhancer-binding protein. *Science*, **275**, 1658–1661.

Edited by W. Baumeister

(Received 24 April 1998; received in revised form 29 July 1998; accepted 4 August 1998)